THE JOURNAL OF PHYSICAL CHEMISTRY A

Article

Cite This: J. Phys. Chem. A 2019, 123, 4964−4972

pubs.acs.org/JPCA

Temperature Dependence of the Reaction of Chlorine Atoms with CH_3OH and CH_3CHO

Aileen O. Hui,*[,†] Mitchio Okumura,*[,†] and Stanley P. Sander*[,‡]

[†]Arthur Amos Noyes Laboratory of Chemical Physics, Division of Chemistry and Chemical Physics, California Institute of Technology, M/S 127-72, 1200 East California Boulevard, Pasadena, California 91125, United States

[‡]Jet Propulsion Laboratory, California Institute of Technology, 4800 Oak Grove Drive, Pasadena, California 91109, United States

Supporting Information

ABSTRACT: Rate constants of the reactions Cl + CH_3OH → CH_2OH + HCl (k_1) and Cl + CH_3CHO → $CH_3C(O)$ + HCl (k_3) were measured at 100 Torr over the temperature range 230.3−297.1 K. Radical chemistry was initiated by pulsed laser photolysis of Cl_2 in mixtures of CH_3OH and CH_3CHO in a flow reactor. Heterodyne near-IR wavelength modulation spectroscopy was used to directly detect HO_2 produced from the subsequent reaction of CH_2OH with O_2 in real time to determine the rate of reaction of Cl with CH_3OH. The rate of Cl + CH_3CHO was measured relative to that of the Cl + CH_3OH reaction. Secondary chemistry, including that of the adducts HO_2·CH_3OH and HO_2·CH_3CHO, was taken into account. The Arrhenius expressions were found to be $k_1(T) = 5.02^{+1.8}_{-1.5} \times 10^{-11} \exp[(20 \pm 88)/T]$ cm^3 molecule^{-1} s^{-1} and $k_3(T) = 6.38^{+2.4}_{-2.0} \times 10^{-11} \exp[(56 \pm 90)/T]$ cm^3 molecule^{-1} s^{-1} (2σ uncertainties). The average values of the rate constants over this temperature range were $k_1 = (5.45 \pm 0.37) \times 10^{-11}$ cm^3 molecule^{-1} s^{-1} and $k_3 = (8.00 \pm 1.27) \times 10^{-11}$ cm^3 molecule^{-1} s^{-1} (2σ uncertainties), consistent with current literature values.

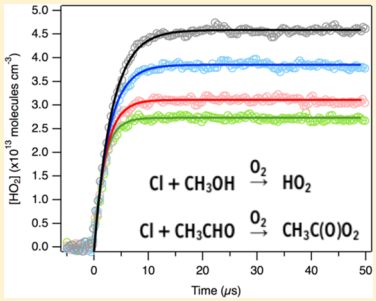

INTRODUCTION

Organic free radicals are ubiquitous intermediates in the Earth's troposphere, formed from the oxidation of volatile organic compounds (VOCs). Due to their key roles in air quality, oxidation reactions that generate free radicals are of great interest in atmospheric chemistry. Although OH is the primary daytime oxidant, Cl atoms can be the major oxidant locally in certain regions, such as in the marine boundary layer.[1−3] Furthermore, Cl atoms may be more ubiquitous than previously assumed;[4−9] Raff et al.[10] have recently proposed that Cl atoms may be generated from the photolysis of $ClNO_2$ formed by heterogeneous reactions.

CH_3OH and CH_3CHO are two major components of oxygenated volatile organic compounds in the troposphere. They are biogeochemically active and serve as tracers of biogenic emission. CH_3OH is present throughout the atmosphere and is the second most abundant VOC after CH_4.[11] CH_3CHO is a primary pollutant produced from ethanol combustion and is also formed from the photo-oxidation of VOCs.[12−14] In the atmosphere, their reactions with Cl atoms are followed rapidly by reaction with O_2 to form peroxy radicals (HO_2 and $CH_3C(O)O_2$)

$$Cl + CH_3OH \rightarrow CH_2OH + HCl \quad (R1)$$

$$CH_2OH + O_2 \rightarrow HO_2 + CH_2O \quad (R2)$$

$$Cl + CH_3CHO \rightarrow CH_3C(O) + HCl \quad (R3)$$

$$CH_3C(O) + O_2 \xrightarrow{M} CH_3C(O)O_2 \quad (R4)$$

Accurate characterization of the rate constants of R1 and R3 (k_1 and k_3, respectively) over an atmospherically relevant range of temperatures is thus important in modeling CH_3OH and CH_3CHO chemistry in regions of the troposphere where Cl-atom oxidation dominates. In the laboratory, Cl atoms are commonly used to generate free radicals. The reactions of Cl atoms with CH_3OH (R1) and CH_3CHO (R3) have been widely used to source hydroperoxy (HO_2) and acetylperoxy ($CH_3C(O)O_2$) radicals, respectively. Both reactions have been used simultaneously in studies of the kinetics and product yields of the HO_2 + $CH_3C(O)O_2$ cross-reaction.[15−24] The accuracy in the experimentally determined kinetics parameters of reactions such as HO_2 + $CH_3C(O)O_2$ is limited in part by the uncertainties in k_1 and k_3.

Numerous room-temperature studies have measured k_1[25−32] and k_3[26,29−31,33−37] using relative and absolute rate methods, with consistent results in the reported values. However, the temperature dependences of R1 and R3 are not as well defined. Although k_1 has been extensively investigated over a wide range of temperatures,[38−41] there are disagreements among the different studies. The direct study by Michael et al.[38] reported k_1 to be temperature-independent over the temperature range T = 200−500 K and was consistent with the indirect study by Lightfoot et al.[39] (T = 248−573 K). On the other hand, the work by Garzón et al.[40] suggested that k_1 has a significant temperature dependence over the range T = 266−380 K.

Received: January 2, 2019
Revised: May 1, 2019
Published: May 15, 2019

DOI: 10.1021/acs.jpca.9b00038
J. Phys. Chem. A 2019, 123, 4964−4972

Meanwhile, Kaiser and Wallington[41] reported a weaker temperature dependence over the range T = 291−475 K using relative rate (RR) measurements. The JPL data evaluation has not recently reevaluated k_1 and is current only up to the JPL02-25 recommendation in 2003.[42] Thus, the JPL evaluation does not include the more recent works by Garzón et al.[40] and Kaiser and Wallington[41] and recommends k_1 to be temperature-independent.[42] The IUPAC evaluation suggests that Garzón et al.[40] may have overestimated the activation barrier and also excludes the results from Garzón et al.[40] in their recommendations;[43] however, a small temperature dependence for k_1 is recommended based on the work by Kaiser and Wallington.[41]

The temperature dependence of k_3 has only been investigated once by Payne et al.,[44] whose results showed that k_3 was temperature-independent over the range T = 210−343 K. Their measured value of k_3= (6.6 ± 1.4) × 10^{-11} cm^3 $molecule^{-1}$ s^{-1} was on the lower range of the values reported by other previous measurements at room temperature, albeit still within the uncertainty limits. The IUPAC data evaluation recommends k_3 to be temperature-independent based on the single study, and there is currently no recommendation for k_3 in the JPL evaluation.

The diverse experimental techniques used in previous measurements of k_1 and k_3 include both absolute and relative rate methods. A majority of the previous studies obtained kinetics data by directly or indirectly monitoring the rate of disappearance of the reactants (i.e., CH_3OH,[26,27,29,41] CH_3CHO,[26,29,33−35] or Cl atoms[25,28,29,32,38,40,44]). The accuracy of the rate constants determined from relative rate methods is generally limited by the reference reaction as well as by other reactions that competitively remove the measured reagents (i.e., CH_3OH and/or CH_3CHO). Resonance fluorescence (RF) techniques offer high sensitivity to Cl atoms but require proper characterization of additional losses such as wall reactions, quenching, and diffusion.

A few studies have used product detection to determine the rate constants (e.g., HCl product from R1[30,31] and R3[30,31,36]) but were only carried out at room temperature. A recent work by Howes et al.[37] demonstrated that accurate measurement of k_3 could be obtained by monitoring the $CH_3C(O)$ product using photoionization mass spectrometry (MS). A value of k_3 = (7.7 ± 0.7) × 10^{-11} cm^3 $molecule^{-1}$ s^{-1} at room temperature was reported, in excellent agreement with the IUPAC recommendations.

In this work, we measured k_1 and k_3 by detecting the HO_2 product formed via R2. Cl atoms were generated using pulsed laser photolysis (PLP), and HO_2 was monitored in the near-IR (NIR) in real time using IR 2f wavelength modulation spectroscopy (WMS). The main advantage of our technique was our high sensitivity to HO_2 radicals and a well-defined overlap between the photolysis volume and the detected radical product. The temperature dependences of k_1 and k_3 were determined over the temperature range 230.3−297.1 K at 100 Torr in N_2. Gas mixtures containing $Cl_2/O_2/N_2/CH_3OH$ or $Cl_2/O_2/N_2/CH_3CHO$ were used to determine k_1 and k_3, respectively, using pseudo-first-order kinetics. All experiments were carried out under conditions where the O_2, CH_3OH, and CH_3CHO concentrations were all in excess relative to Cl atoms.

EXPERIMENTAL METHODS

The infrared kinetics spectroscopy (IRKS) apparatus consisted of a temperature-controlled pulsed laser photolysis flow cell coupled to simultaneous IR and UV absorption spectroscopy and has been described in detail previously.[45−47] Only the details pertinent to the present work will be provided, including modifications that were made since the last publication.

The flow cell was a jacketed Pyrex cell of length 175 cm and diameter 5 cm and was temperature-controlled by flowing liquid nitrogen-cooled methanol circulating through the jacket of the cell. The temperature was measured with a calibrated type T thermocouple (Omega) inserted into the jacket of the cell. This temperature measurement was consistent with in situ measurements made inside of the cell. The temperature profile along the length of the cell was verified to be uniform across the volume probed by the IR laser. Reagent gases were premixed and precooled in a Pyrex manifold prior to entering the cell. Room-temperature N_2 purge gas flowed from the aluminum chambers on either end of the cell toward the gas pump-out ports to confine the main gas flow to the temperature-controlled region and to protect the Herriott mirrors that formed the multipass optical cavity for the IR probes. The gas flows were regulated by mass flow controllers (MKS Instruments), and the total flow rate was kept at approximately 2000 cm^3 (STP) min^{-1}, maintaining a 10 s residence time inside the flow cell at a total pressure of 100 ± 2 Torr. CH_3OH and CH_3CHO were introduced into the cell by flowing N_2 through glass bubblers containing the liquid compounds, held inside temperature-controlled baths. The pressures in the reaction cell and bubblers were measured by absolute capacitance pressure gauges (MKS Baratron), and the concentrations of CH_3OH and CH_3CHO vapors were determined from their flow rates using the known vapor pressures of the pure compounds and assuming complete saturation in the bubblers.

Light (351 nm) from a XeF excimer laser (Compex 301) operating in the constant energy mode was directed coaxially through the flow cell to initiate the chemistry by photolyzing Cl_2 molecules in gas mixtures of $Cl_2/N_2/O_2/CH_3OH/CH_3CHO$. A photolysis repetition rate of 0.2 Hz was used, resulting in two photolysis events occurring per residence time. Decreasing the repetition rate to 0.1 Hz made no difference in the kinetics traces. At repetition rates above 0.2 Hz, we observed small changes in the kinetics traces due to possible photolysis of reaction products. For this reason, the repetition rates were limited to 0.2 Hz and below.

All experiments were conducted using excess concentrations of O_2, CH_3OH, and CH_3CHO relative to the initial radical concentrations ($[Cl]_0$), such that all Cl atoms generated from photolysis were assumed to form either HO_2 or $CH_3C(O)O_2$ via R1 and R3, respectively. Typical concentrations of the reagents were $[CH_3OH]$ = (2.4−10.7) × 10^{15} molecules cm^{-3}, $[CH_3CHO]$ = (0.9−8.4) × 10^{15} molecules cm^{-3}, $[O_2]$ = (1.6−2.0) × 10^{18} molecules cm^{-3}, and $[Cl_2]$ = (0.8−5.3) × 10^{15} molecules cm^{-3}, with total radical concentrations of $[Cl]_0$ = (1.8−19) × 10^{13} molecules cm^{-3}.

A 3 mW continuous-wave distributed feedback laser operating in the NIR was used for sensitive detection of HO_2 radicals. The diode laser was tuned to the rovibrational transitions of the first overtone of the O—H stretch of HO_2 ($2\nu_1$: 6638.2 cm^{-1}). The laser output was wavelength

DOI: 10.1021/acs.jpca.9b00038
J. Phys. Chem. A 2019, 123, 4964−4972

modulated at 6.8 MHz by sinusoidally modulating the injection current with an external function generator. 2*f*-Heterodyne detection was implemented by demodulating the detected signal at 13.6 MHz. The demodulated signal was collected at a sampling rate of 2.5 MHz, amplified by a factor of 200, and low-pass filtered at 1 MHz using a low-noise preamplifier (SRS SR560). The noise-equivalent concentration per $Hz^{-1/2}$ of HO_2 normalized to one excimer shot was 2.9×10^9 molecules cm^{-3} $Hz^{-1/2}$. For a typical experimental run, the HO_2 signal was averaged for 65−75 excimer laser shots, and the minimum detectable concentration of HO_2 was $\sim 4 \times 10^{10}$ molecules cm^{-3}. Although we had the sensitivity to perform the experiment at lower overall radical concentrations, the higher concentration provided better signal-to-noise ratios, and under our conditions, did not further complicate the kinetics.

Since WMS only measures the relative changes in the concentration, the NIR laser was calibrated daily to obtain absolute concentrations of HO_2. The NIR laser was calibrated against UV absorption at $\lambda = 225$ nm ($\sigma_{HO_2} = 2.88 \times 10^{-18}$ cm^2 $molecule^{-1}$) by measuring the NIR and UV decay signals simultaneously when HO_2 was the only peroxy radical present; i.e., $[CH_3CHO] = 0$. This calibration procedure has been used previously and is described in more detail elsewhere.[15] A thorough discussion and comparison of other HO_2 calibration methods can also be found in Onel et al.[48] Broadband UV light was provided by a laser-driven light source (Energetiq EQ-99XFC). The collimated UV beam was coaligned with and counter-propagated the excimer beam, making a single pass through the cell. A monochromator (Acton Research Corporation Spectra Pro-300i) placed in front of a photomultiplier tube was used for the wavelength-specific detection of the transmitted UV light. Baffles were placed on both ends of the flow cell to ensure that only light that sampled the photolysis volume entered the monochromator. Despite a different geometric overlap due to the off-axis orientation of the Herriott mirrors, the IR and UV probe beams should capture the same physical processes at relatively short time scales (<20 ms); i.e., before diffusion becomes a significant loss process. At the beginning of every experiment, the kinetics traces from the HO_2 self-reaction were collected at three different initial radical concentrations at room temperature. The IR and UV traces were simultaneously fit to a bimolecular decay using the kinetics modeling program, FACSIMILE,[49] to obtain the calibration factor, which converts the IR signal in mV to the absolute HO_2 concentration.

RESULTS AND DISCUSSION

As mentioned previously, all experiments were conducted using excess $[O_2]$, $[CH_3OH]$, and $[CH_3CHO]$ relative to $[Cl]_0$. $[O_2]$ was in excess of $[Cl]_0$ by at least a factor of 10^4, and $[CH_3OH]$ and $[CH_3CHO]$ were typically in excess of $[Cl]_0$ by at least a factor of 20. Kinetics modeling showed that under these conditions, the ratios of $[Cl]_0$ to $[O_2]$, $[CH_3OH]$, and $[CH_3CHO]$ had no effect on the returned values of k_1 and k_3. $[O_2]$ was also in excess of both $[CH_3OH]$ and $[CH_3CHO]$, such that the first-order loss rates of R2 and R4 were at least 10 times greater than both R1 and R3. For example, at the lowest O_2 concentration ($[O_2] = 1.6 \times 10^{18}$ molecules cm^{-3}) and highest CH_3OH and CH_3CHO concentrations ($\sim 1 \times 10^{16}$ molecules cm^{-3}), the first-order loss rates were

$$k_2[O_2] \sim 8 \times 10^6\ s^{-1} \approx 15k_1[CH_3OH] \approx 14k_3[CH_3CHO] \quad (1)$$

$$k_4[O_2] \sim 1 \times 10^8\ s^{-1} \approx 160k_1[CH_3OH] \approx 150k_3[CH_3CHO] \quad (2)$$

where

$$k_2 \sim 9.1 \times 10^{-11} cm^3\ molecule^{-1}\ s^{-1}\ (\text{ref: JPL15-10}^{42}) \quad (3)$$

$$k_4 \sim 5.1 \times 10^{-12} cm^3\ molecule^{-1}\ s^{-1}\ (\text{ref: Atkinson et al.}^{50}) \quad (4)$$

$$k_1 \sim 5.5 \times 10^{-11} cm^3\ molecule^{-1}\ s^{-1}\ (\text{ref: JPL 15-10}^{42}) \quad (5)$$

$$k_3 \sim 8.0 \times 10^{-11} cm^3\ molecule^{-1}\ s^{-1}\ (\text{ref: IUPAC}^{43}) \quad (6)$$

Thus, the rate-limiting steps for the formation of HO_2 and $CH_3C(O)O_2$ can be approximated to be R1 and R3, respectively; i.e.,

$$Cl + CH_3OH \rightarrow HO_2 \quad (R5)$$

$$Cl + CH_3CHO \rightarrow CH_3C(O)O_2 \quad (R6)$$

The formation of HO_2 and $CH_3C(O)O_2$ were pseudo-first-order since both $[CH_3OH]$ and $[CH_3CHO]$ were in excess relative to $[Cl]_0$; therefore, the rate law for HO_2 can be written as

$$\frac{d[HO_2]}{dt} = k_1[CH_3OH][Cl]_0 \times \exp[-(k_1[CH_3OH] + k_3[CH_3CHO])t] \quad (7)$$

$$= k_1'[Cl]_0 \exp[-(k_1' + k_3')t] \quad (8)$$

where k_1' and k_3' are the pseudo-first-order rate constants for R1 and R3, respectively; i.e.,

$$k_1' = k_1[CH_3OH] \quad (9)$$

and

$$k_3' = k_3[CH_3CHO] \quad (10)$$

Experimental conditions were chosen to minimize subsequent losses of HO_2 via the self-reaction (R7) and reaction with $CH_3C(O)O_2$ (R8).

$$HO_2 + HO_2 \xrightarrow{M} H_2O_2 + O_2 \quad (R7)$$

$$HO_2 + CH_3C(O)O_2 \rightarrow \text{products} \quad (R8)$$

This was achieved by using sufficiently low initial radical concentrations such that the decrease in the HO_2 signal from $\sim$20−30 μs (i.e., after the conversion of Cl to HO_2 and $CH_3C(O)O_2$ was completed) to $\sim$50 μs was less than 5%.

At low temperatures, the range of experimental conditions that could be explored was additionally limited by the need to minimize the rapid loss of HO_2 by reaction with CH_3OH and/or with CH_3CHO via R9 and R10, respectively, such that eq 8 was still valid.

$$HO_2 + CH_3OH \underset{M}{\overset{M}{\rightleftarrows}} HO_2 \cdot CH_3OH \quad (R9)$$

$$HO_2 + CH_3CHO \underset{M}{\overset{M}{\rightleftarrows}} HO_2 \cdot CH_3CHO \quad (R10)$$

DOI: 10.1021/acs.jpca.9b00038
J. Phys. Chem. A 2019, 123, 4964−4972

The formation of the hydrogen-bonded adducts via R9 and R10 becomes more favored at lower temperatures. Previous studies have also shown that these adducts introduce additional loss processes for HO_2 via R11 and R12, resulting in an enhanced observed HO_2 decay rate that becomes more significant at lower temperatures, even at relatively low CH_3OH and CH_3CHO concentrations.[51]

$$HO_2 + HO_2{\cdot}CH_3OH \rightarrow \text{products} \quad \text{(R11)}$$

$$HO_2 + HO_2{\cdot}CH_3CHO \rightarrow \text{products} \quad \text{(R12)}$$

Therefore, $[CH_3OH]$ and $[CH_3CHO]$ were typically limited to less than $\sim 1 \times 10^{16}$ molecules cm^{-3} and $\sim 5 \times 10^{15}$ molecules cm^{-3}, respectively, for temperatures below T = 250 K to minimize the adduct formation and rapid loss of HO_2. Using the previously determined equilibrium constants for R9 and R10,[52] the upper limit of the uncertainty in the HO_2 concentration, calculated from the highest $[CH_3OH]$ and $[CH_3CHO]$ used, was ~2% at T = 297.1 K and ~20% at T = 230.3 K.

Rate Constant of Cl + CH_3OH (k_1). R1 was investigated by measuring the formation signal of HO_2 in the absence of CH_3CHO at various concentrations of CH_3OH. In the absence of CH_3CHO, the integrated rate law for HO_2 is given by eq 11

$$[HO_2] = [Cl]_0 - [Cl]_0 e^{-k_1' t} \quad (11)$$

The data were fit with a single exponential function with an effective rate constant, k_1', as given by eq 9. The data were fit from $t \sim 1.6$ to ~50 μs. The data points for $t < 1.6$ μs were susceptible to electrical pick-up from the excimer pulse and were thus excluded from the fit. The fitted curves extrapolated to $t = 0$ showed that the data curves were well defined by eq 11.

The HO_2 formation curves measured at T = 297.1 K and at T = 230.3 K using varying $[CH_3OH]$ are shown in Figure 1a and 1b, respectively. The fits to the data are shown in solid lines, and the extrapolations to $t = 0$ are represented by dashed lines. Both figures demonstrate that the HO_2 formation rate increases with increasing $[CH_3OH]$, as expected. The observed $[HO_2]$ from the lowest $[CH_3OH]$ (blue markers) in Figure 1b is approximately 5% higher than the $[Cl]_0$; however, this is within the 10% uncertainty in the calibration of the NIR signal. Details on the error analysis of our calibration methods can be found elsewhere.[15] Briefly, the systematic error in the NIR calibration was determined by running Monte Carlo simulations of the simultaneous IR and UV fits. These calculations accounted for uncertainties in the UV absorption cross-sections of HO_2, H_2O_2, k_7 and the unimolecular diffusion rate constants.

Figure 1a shows that at room temperature, the HO_2 signals level off to a common value by ~50 μs, indicating complete conversion of Cl to HO_2 without significant subsequent loss of HO_2 via reaction with $[CH_3OH]$ (R9). On the other hand, the HO_2 signals in Figure 1b do not level off to the same value; rather, the yields of HO_2 appear to decrease with increasing $[CH_3OH]$. The negative dependence of the HO_2 yield on $[CH_3OH]$ is attributed to the rapid loss of HO_2 from the formation of the hydrogen-bonded adduct with CH_3OH (R9). This effect was evident at temperatures below 250 K for $[CH_3OH] > 1 \times 10^{16}$ molecules cm^{-3}, which was used as the upper limit of the range of $[CH_3OH]$ that was used so that eq 11 was still valid. $[Cl]_0$ was also kept below 1×10^{14} molecules cm^{-3} for $T < 250$ K to decrease the HO_2 loss rate; at T = 230.3 K, however, rapid loss of HO_2 could not completely be avoided even at the lowest $[Cl]_0$ and $[CH_3OH]$ conditions. Based on the equilibrium constant of R9 determined previously,[52] approximately 15% of HO_2 is predicted to be complexed at the highest $[CH_3OH] = 8.5 \times 10^{15}$ molecules cm^{-3}. For data collected at lower temperatures and at high $[CH_3OH]$, the number of data points in the kinetics traces that were used in the fits was reduced to minimize capturing the fast HO_2 loss via R9. The additional error introduced by reducing the sample size effectively accounted for the uncertainties in the fitted $[HO_2]$ assuming no subsequent loss. A subset of the data was also analyzed using methods that took into account the subsequent HO_2 removal via either pseudo-first-order or second-order loss processes (Supporting Information). The fitted values of the rate constants in both cases were consistent with the results obtained using the simplified pseudo-first-order growth model described here.

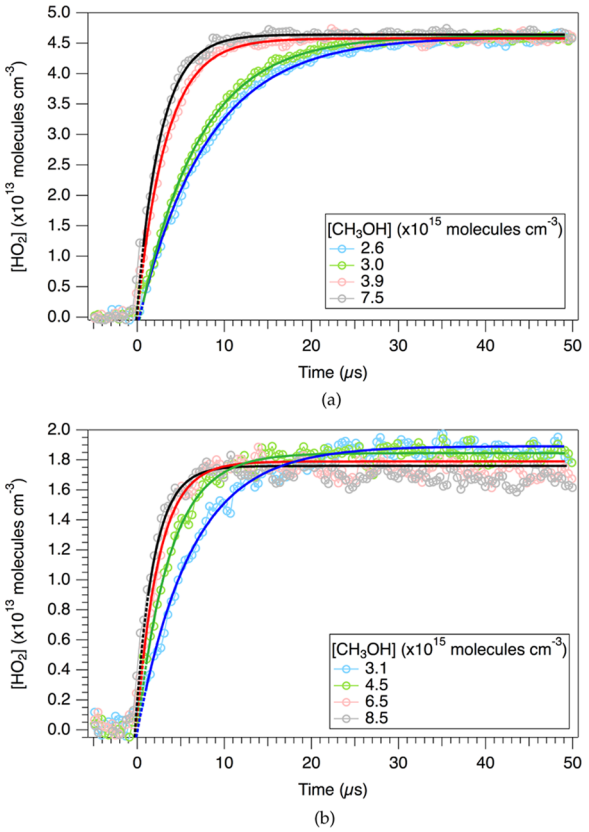

Figure 1. Example data demonstrating pseudo-first-order growths of HO_2 using varying $[CH_3OH]$ with $[CH_3CHO] = 0$ at (a) T = 294.8 K, $[Cl]_0 = 4.6 \times 10^{13}$ molecules cm^{-3}, and (b) T = 230.3 K, $[Cl]_0 = 1.8 \times 10^{13}$ molecules cm^{-3}. Dashed lines are the fits extrapolated to $t = 0$.

The measured values of k_1' at each temperature were plotted against $[CH_3OH]$, and total linear least-squares regressions to the data were used to determine k_1. The pseudo-first-order plots of R1 at three temperatures are shown in Figure 2. The fitted values of k_1 are tabulated in Table 1 along with the range of experimental conditions that were used to measure k_1'. The uncertainties in k_1 (2σ) include the random errors in k_1' (typical: ~1−2%, maximum: ~10%) as well as systematic errors in the pressures, flows, and temperatures (total uncertainty in $[CH_3OH]$: ~ 2.5%).

DOI: 10.1021/acs.jpca.9b00038
J. Phys. Chem. A 2019, 123, 4964−4972

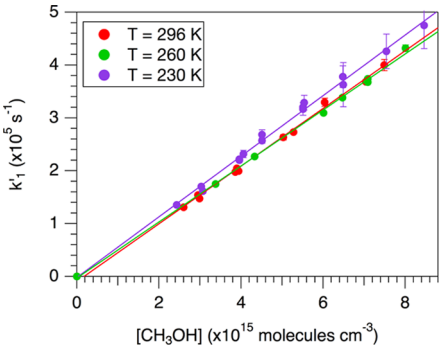

Figure 2. Plot of k_1 as a function of CH_3OH at T = 230.3 K, 260.1 K, and 297.1 K.

The Arrhenius expression was found to be $k_1(T) = 5.02^{+1.8}_{-1.5} \times 10^{-11} \exp[(20 \pm 88)/T]$ cm^3 molecule^{-1} s^{-1}. Within experimental uncertainty, the rate constant was temperature-independent over the temperature range 230.3−297.1 K, which is consistent with the results from Michael et al.[38] and Lightfoot et al.[39] An average value of $k_1 = (5.45 \pm 0.37) \times 10^{-11}$ cm^3 molecule^{-1} s^{-1} (2σ uncertainty) was determined from the values measured at each temperature weighted by the corresponding uncertainties. Table 2 compares the results from this work with those of previous works in the literature. The results are in excellent agreement with the room-temperature values from previous measurements and with the JPL and IUPAC recommendations. k_1 was observed to lack a significant temperature dependence, further challenging the previous results by Garzón et al.[40] Kaiser and Wallington[41] reported a weak temperature dependence for temperatures at and above room temperature, which are beyond the range of temperatures that was studied in this work. Nonetheless, extrapolation of the data from Kaiser and Wallington[41] to lower temperatures results in values that are smaller than our measured values of k_1.

The uncertainty in the average value of k_1 is the weighted standard deviation and includes both random errors in the fits and systematic errors in the measured concentrations of $[CH_3OH]$; systematic errors from secondary chemistry are not included. Under the conditions of these experiments, loss of HO_2 from R7 is estimated to be less than 5% across all temperatures, contributing to less than 10% error in the fitted values of k_1'. For temperatures below 250 K, the loss of HO_2 via R11 becomes more significant; at T = 230.3 K, this is estimated to introduce between 1 and 30% error to k_1' at the lowest and largest $[CH_3OH]$, respectively.

Rate Constant of Cl + CH_3CHO (k_3). In the presence of CH_3CHO, a fraction of the Cl radicals is lost via R3, and the integrated rate law for HO_2 is given by eq 12

$$[HO_2] = \left(\frac{k_1'}{k_{eff}}\right)[Cl]_0(1 - e^{-k_{eff}t}) \quad (12)$$

where

$$k_{eff} = k_1' + k_3' \quad (13)$$

k_3' was measured at each temperature for varying concentrations of CH_3OH and CH_3CHO. Example traces of HO_2 in the presence of both CH_3OH and CH_3CHO at two different temperatures are shown in Figure 3. For each temperature, the HO_2 profile obtained in the absence of CH_3CHO is provided for reference. In Figure 3a and 3b, the HO_2 traces do not level off to a common value due to the additional loss of Cl via R6. Each HO_2 time profile was fit to eq 12, allowing the pre-exponential factor, $A = k_1'[Cl]_0/k_{eff}$, and k_{eff} in the exponent to be varied parameters. The long-time HO_2 level (i.e., $t \sim 25-50$ μs), which is defined by the pre-exponential factor, A, could also be used to estimate k_{eff} without fitting the data with eq 12. These estimates of k_{eff} were found to be self-consistent with the values of k_{eff} obtained from the fit.

For data sets where $[CH_3CHO]$ was varied for a fixed $[CH_3OH]$, it was confirmed that the intercept of the linear fit to k_{eff} vs $[CH_3CHO]$ yielded $k_1[CH_3OH]$, where k_1 was consistent, within experimental uncertainty, with the measured value of 5.45×10^{-11} cm^3 molecule^{-1} s^{-1} (Table 2). From eq 13, k_3' was calculated using the value of k_1 determined in this work. Figure 4 shows a plot of k_3' versus $[CH_3CHO]$ for three different temperatures. Data from all other temperatures were revealed to have similar linear dependences and have been excluded in the figure for clarity. Values of k_3 at each temperature were determined from the slopes of the linear fits to the data.

The average values of k_3 determined at each temperature and the range of precursor and initial radical concentrations that were used are summarized in Table 3. The uncertainties in k_3 (2σ) include the random errors in k_3' (typical: ∼2−3%, maximum: ∼10%) as well as systematic errors in k_{eff} and in the pressures, flows, and temperatures (total uncertainty in $[CH_3CHO]$: ∼ 5%).

The Arrhenius expression was found to be $k_3(T) = 6.38^{+2.4}_{-2.0} \times 10^{-11} \exp[(56 \pm 90)/T]$ cm^3 molecule^{-1} s^{-1}. Similarly to R1, R3 was revealed to have no discernible temperature dependence in the temperature range T = 230.3−297.1 K, with an average value of $k_3 = (8.00 \pm 1.27) \times 10^{-11}$ cm^3 molecule^{-1} s^{-1} (2σ uncertainty). The uncertainty is the weighted standard

Table 1. Experimental Conditions for the Determination of k_1[a]

T (K)	$[O_2]$ (×10^{18} cm^{-3})	$[Cl_2]$ (×10^{15} cm^{-3})	$[CH_3OH]$ (×10^{15} cm^{-3})	$[Cl]_0$ (×10^{13} cm^{-3})	k_3 (×10^{-11} cm^3 s^{-1})
297.1	1.58	5.29	2.99−8.84	19	5.58 ± 0.36
294.8	1.58	1.49	2.60−7.49	4.6	5.53 ± 0.42
280.2	1.66	1.56−3.8	2.98−8.01	5.1−13	5.21 ± 0.32
269.8	1.72	1.20−2.44	2.45−9.13	5.2−9.1	5.44 ± 0.28
260.1	1.79	1.68−3.8	3.38−8.01	6.0−12	5.33 ± 0.34
250.4	1.86	1.93−5.29	5.21−12.1	7.0−18	5.42 ± 0.30
240.3	1.93	1.82−3.8	2.95−6.47	5.0−9.0	5.39 ± 0.46
230.3	2.02	0.75−1.90	2.43−8.46	1.8−5.2	5.99 ± 0.42

[a]Uncertainties in k_1 are 2σ.

DOI: 10.1021/acs.jpca.9b00038
J. Phys. Chem. A 2019, 123, 4964−4972

Table 2. Comparison of Measured k_1 with the Literature Values

ref	T (K)	P (Torr)	k_1[a] ($\times 10^{-11}$ cm^3 s^{-1})	method[b]
Michael et al.[38]	200−500	760	6.33 ± 1.40	FP/RF
Payne et al.[25]	298	1	5.1 ± 1.0	DF/MS
Wallington et al.[26]	295	760	4.57 ± 0.40	RR/UVP/GC[c]
Lightfoot et al.[39]	248−573	210−760	5.3 ± 2.4	RR/FP/UVA[d]
Nelson et al.[27]	298	730−750	4.79 ± 0.36	RR/UVP/GC[e]
Dóbé et al.[28]	298	1.35	6.14 ± 1.33	DF/EPR
Tyndall et al.[29]	295	700	5.1 ± 0.4	PLP/RF
			5.6 ± 0.6	RR/PLP/RF[c,f]
Smith et al.[30]	295	10	5.6 ± 0.2	PLP/IR
Seakins et al.[31]	298	25	5.83 ± 0.77	PLP/IR
			5.38 ± 0.25	PLP/CL
Taketani et al.[32]	295	3	5.35 ± 0.24	PLP/LIF
Garzón et al.[40]	264−382	20−200	(35.5 ± 2.2) exp[−(559 ± 40)/T]	PLP/RF
Kaiser and Wallington[41]	291−475		(8.6 ± 1.3) exp[−(167 ± 60)/T]	RR/UVP/GC[c]
this work	230.3−297.1	100	5.45 ± 0.37	PLP/IR
JPL[42]	200−573		5.5[g]	
IUPAC[43]	200−500		7.1 exp(−75/T)[h]	

[a]Errors are 2σ. [b]FP = flash photolysis; DF = discharge flow; PLP = pulsed laser photolysis; UVP = UV photolysis; MS = mass spectrometry; GC = gas chromatography; UVA = UV absorption; EPR = electron paramagnetic resonance; RF = resonance fluorescence; IR = IR absorption; CL = chemical luminescence; LIF = laser-induced fluorescence; FTIR = Fourier transform IR spectroscopy; RR= relative rate. [c]Reference reaction: Cl + C_2H_6; k_{ref} = 5.7 × 10^{-11} cm^3 molecule^{-1} s^{-1}. [d]Cl + CH_4; k_{ref} = 1.0 × 10^{-13} cm^3 molecule^{-1} s^{-1}. [e]Cl + c-C_6H_{12}; k_{ref} = 3.11 × 10^{-10} cm^3 molecule^{-1} s^{-1}. [f]Reference reaction: Cl + C_2H_4; k_{ref} = 9.3 × 10^{-11} cm^3 molecule^{-1} s^{-1}. [g]$\Delta \log_{10} k(298\ \mathrm{K}) = 1.2$, $\Delta(E/R) = \pm 100$ K. [h]$\Delta \log_{10} k(298\ \mathrm{K}) = 0.07$, $\Delta(E/R) = \pm 200$ K.

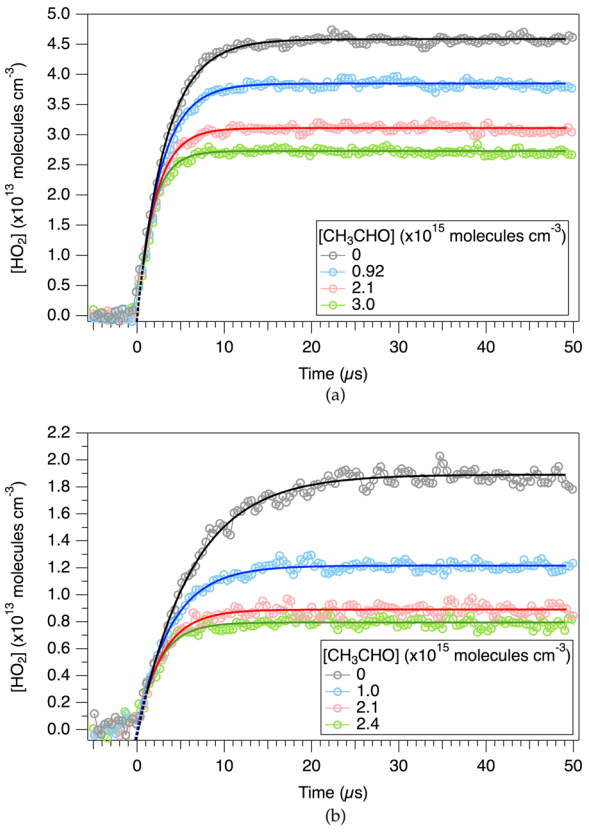

Figure 3. Example data demonstrating pseudo-first-order growths of HO_2 using varying [CH_3CHO] with fixed [CH_3OH] at (a) T = 294.8 K, $[Cl]_0$ = 4.6 × 10^{13} molecules cm^{-3}, [CH_3OH] = 6.1 × 10^{15} molecules cm^{-3}, and (b) T = 230.3 K, $[Cl]_0$ = 1.8 × 10^{13} molecules cm^{-3}, [CH_3OH] = 3.1 × 10^{13} molecules cm^{-3}. Dashed lines are the fits extrapolated to t = 0.

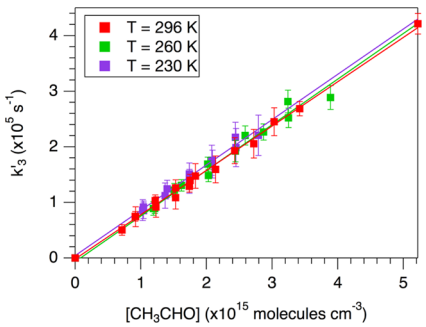

Figure 4. Plot of k_3 as a function of CH_3CHO at T = 230, 260, and 297 K shown with linear fits. All other temperatures have been excluded for clarity. Total linear regression.

deviation and includes both systematic and random errors. This is in excellent agreement with previous measurements and with the IUPAC recommendation (Table 4). Our conclusion that k_3 has no significant temperature dependence over our experimental temperature range is consistent with the only previous temperature-dependence study by Payne et al.[44] Although our value of k_3 is higher than that reported by Payne et al.,[44] our results are still within their 2σ uncertainty bounds.

As mentioned in previous works by Michael et al.[38] and Payne et al.,[44] the temperature dependence of hydrogen abstraction reactions of related oxygenated hydrocarbons by Cl can be predicted based on the R−H bond energies. Specifically, hydrogen abstraction reactions by Cl for R−H molecules with bond energies between those of C_2H_6 (98 kcal mol^{-1}) and CH_2O (86 kcal mol^{-1}) are expected to be temperature-independent, based on the observation that C_2H_6 and CH_2O were, respectively, found to have minimal to no temperature dependence in their reactions with Cl. The bond energies for the C−H bond in CH_3OH and in the aldehydic C−H bond in CH_3CHO are both ∼95 kcal mol^{-1}.[53−55] Based on the empirical correlation between the R−H bond energies

DOI: 10.1021/acs.jpca.9b00038
J. Phys. Chem. A 2019, 123, 4964−4972

Table 3. Experimental Conditions for the Determination of k_3[a]

T (K)	$[O_2]$ ($\times 10^{18}$ cm^{-3})	$[Cl_2]$ ($\times 10^{15}$ cm^{-3})	$[CH_3OH]$ ($\times 10^{15}$ cm^{-3})	$[CH_3CHO]$ ($\times 10^{15}$ cm^{-3})	$[CH_3OH]/[CH_3CHO]$	$[Cl]_0$ ($\times 10^{13}$ cm^{-3})	k_3 ($\times 10^{-11}$ cm^3 s^{-1})
297.1	1.58	3.02−5.29	3.90	0.71−5.22	2.25−6.60	19	8.16 ± 1.08
294.8	1.58	1.49	3.00−6.08	0.92−3.03	0.75−5.46	4.5	7.61 ± 1.78
280.2	1.66	1.56	2.97−4.99	0.95−1.93	1.87−6.80	5.1−13	7.24 ± 2.34
269.8	1.72	1.61−2.12	4.01−6.06	0.97−5.11	0.97−5.14	5.3−7.5	7.78 ± 1.00
260.1	1.79	1.68	3.44−4.40	1.19−3.89	1.12−3.73	6.0	8.21 ± 1.26
250.4	1.86	1.93−3.53	5.23−6.35	1.26−8.43	0.62−4.14	7.1−1.2	8.11 ± 0.74
240.3	1.93	1.82	2.96−5.98	0.98−4.56	1.31−6.10	5.0	7.95 ± 1.22
230.3	2.02	0.75	3.08−5.10	1.03−2.80	1.45−4.93	1.8	8.16 ± 2.36

[a]Uncertainties in k_3 are 2σ.

Table 4. Comparison of Measured k_3 with the Literature Values

ref	T (K)	P (Torr)	k_3[a] ($\times 10^{-11}$ cm^3 s^{-1})	method[b]
Niki et al.[33]	298	700	7.6 ± 0.4	RR/UVP/FTIR[c]
Wallington et al.[26]	295	760	8.45 ± 0.79	RR/UVP/GC[c]
Bartels et al.[34]	298	0.75	6.0 ± 0.9	RR/DF/MS[c]
Payne et al.[44]	210−343	25−200	6.6 ± 1.4	FP/RF
Scollard et al.[35]	298	730−750	7.9 ± 0.6	RR/UVP/GC[d]
Tyndall et al.[29]	295	700	7.3 ± 0.7	PLP/RF
			8.4 ± 1.0	RR/PLP/RF[c,e]
Kegley-Owen et al.[36]	298	10−50	7.5 ± 0.8	PLP/IR
Smith et al.[30]	295	10	8.3 ± 0.1	PLP/IR
Seakins et al.[31]	298	25	7.7 ± 1.1	PLP/IR
	298		8.8 ± 1.5	PLP/CL
Howes et al.[37]	298	1−2	7.7 ± 0.7	PLP/MS
this work	230.3−297.1	100	8.00 ± 1.27	PLP/IR
IUPAC[43]	210−340		8.0[f]	

[a]Errors are 2σ. [b]FP = flash photolysis; PLP = pulsed laser photolysis; UV = UV photolysis; RF = resonance fluorescence; IR = IR absorption; CL = CL chemical luminescence; FTIR = Fourier transform IR spectroscopy; GC = gas chromatography; MS = mass spectrometry; RR= relative rate. [c]Reference reaction: Cl + C_2H_6; $k_{ref} = 5.7 \times 10^{-11}$ cm^3 molecule^{-1} s^{-1}. [d]Reference reaction: Cl + $(CH_3)_2O$; $k_{ref} = 1.76 \times 10^{-10}$ cm^3 molecule^{-1} s^{-1}. [e]Reference reaction: Cl + C_2H_4; $k_{ref} = 9.3 \times 10^{-11}$ cm^3 molecule^{-1} s^{-1}. [f]$\Delta \log_{10} k(298\ \mathrm{K}) = 0.07$, $\Delta(E/R) = \pm 200$ K.

and the observed temperature dependence of the Cl reactions, R1 and R3 are expected to show no temperature dependence, which is consistent with our results.

CONCLUSIONS

The absolute rate constants of the reactions of Cl atoms with CH_3OH and CH_3CHO have been determined at 100 Torr over the temperature range 230.3−297.1 K by measuring the formation rate of HO_2 in various relative concentrations of CH_3OH and CH_3CHO. The values of the rate constants at room temperature are in excellent agreement with previous measurements and support the current recommendations by the JPL and IUPAC evaluations.

Both k_1 and k_3 were found to be temperature independent over our temperature range, within experimental uncertainty. The lack of a temperature dependence for k_1 is consistent with the previous work by Michael et al.[38] and Lightfoot et al.[39] and challenges the results from Garzón et al.[40] Extrapolation of the results from Kaiser and Wallington[41] to lower temperatures lead to values of k_1 that are lower than our measured values; however, additional experiments that cover temperatures both below and above room temperature are needed for further assessment. The temperature independence of k_3 validates the results from the only temperature dependence of R3 by Payne et al.[44] Our value of k_3 was higher than that reported by Payne et al.[44] but was still within the experimental error.

The results from this work provide experimental data for k_1 and k_3 over a temperature range that is relevant for the Earth's lower atmosphere. Although R1 and R3 are unlikely to play key roles in the atmosphere directly, they are both commonly used to generate peroxy radicals in the laboratory for studying other reactions that are important in the troposphere. Therefore, well-defined values for k_1 and k_3 enable accurate characterization of peroxy radical reactions over a wide range of atmospherically relevant temperatures.

ASSOCIATED CONTENT

Supporting Information

The Supporting Information is available free of charge on the ACS Publications website at DOI: 10.1021/acs.jpca.9b00038.

Comparison of fitted values of k_1 and k_3 using pseudo-first-order approximation and using kinetics model with second-order HO_2 loss; complete list of experimental conditions used for the determination of k_1 and k_3 (PDF)

AUTHOR INFORMATION

Corresponding Authors

*E-mail: aileenh@caltech.edu (A.O.H.).
*E-mail: mo@caltech.edu (M.O.).
*E-mail: stanley.p.sander@jpl.nasa.gov (S.P.S.).

ORCID

Aileen O. Hui: 0000-0003-4217-2698
Mitchio Okumura: 0000-0001-6874-1137

DOI: 10.1021/acs.jpca.9b00038
J. Phys. Chem. A 2019, 123, 4964−4972

Notes

The authors declare no competing financial interest.

■ ACKNOWLEDGMENTS

This research was carried out by the Jet Propulsion Laboratory, California Institute of Technology, under contract with the National Aeronautics and Space Administration (NASA). The authors thank the National Science Foundation (NSF Grant No. CHE-1413712), the NASA Earth and Space Science Fellowship (NESSF), and NASA's Upper Atmospheric Research Program (UARP Grant No. NNX12AE01G) and Tropospheric Chemistry Program for financial support.

■ REFERENCES

(1) Spicer, C. W.; Chapman, E. G.; Finlayson-Pitts, B. J.; Plastridge, R. A.; Hubbe, J. M.; Fast, J. D.; Berkowitz, C. M. Unexpectedly High Concentrations of Molecular Chlorine in Coastal Air. *Nature* **1998**, *394*, No. 353.

(2) Keene, W. C.; Stutz, J.; Pszenny, A. A. P.; Maben, J. R.; Fischer, E. V.; Smith, A. M.; von Glasow, R.; Pechtl, S.; Sive, B. C.; Varner, R. K. Inorganic Chlorine and Bromine in Coastal New England Air during Summer. *J. Geophys. Res.: Atmos.* **2007**, *112*, No. 7689.

(3) Finley, B. D.; Saltzman, E. S. Observations of Cl_2, Br_2, and I_2 in Coastal Marine Air. *J. Geophys. Res.: Atmos.* **2008**, *113*, No. D21301.

(4) Ravishankara, A. R. Are Chlorine Atoms Significant Tropospheric Free Radicals? *Proc. Natl. Acad. Sci. U.S.A.* **2009**, *106*, 13639−13640.

(5) Kercher, J. P.; Riedel, T. P.; Thornton, J. A. Chlorine Activation by N_2O_5: Simultaneous, in Situ Detection of $ClNO_2$ and N_2O_5 by Chemical Ionization Mass Spectrometry. *Atmos. Meas. Tech.* **2009**, *2*, 193−204.

(6) Roberts, J. M.; Osthoff, H. D.; Brown, S. S.; Ravishankara, A. R. N_2O_5 Oxidizes Chloride to Cl_2 in Acidic Atmospheric Aerosol. *Science* **2008**, *321*, 1059.

(7) Osthoff, H. D.; Roberts, J. M.; Ravishankara, A. R.; Williams, E. J.; Lerner, B. M.; Sommariva, R.; Bates, T. S.; Coffman, D.; Quinn, P. K.; Dibb, J. E.; et al. High Levels of Nitryl Chloride in the Polluted Subtropical Marine Boundary Layer. *Nat. Geosci.* **2008**, *1*, 324−328.

(8) Behnke, W.; George, C.; Scheer, V.; Zetzsch, C. Production and Decay of $ClNO_2$ from the Reaction of Gaseous N_2O_5 with NaCl Solution: Bulk and Aerosol Experiments. *J. Geophys. Res.: Atmos.* **1997**, *102*, 3795−3804.

(9) Finlayson-Pitts, B. J.; Ezell, M. J.; Pitts, J. N. Formation of Chemically Active Chlorine Compounds by Reactions of Atmospheric NaCl Particles with Gaseous N_2O_5 and $ClONO_2$. *Nature* **1989**, *337*, No. 241.

(10) Raff, J. D.; Njegic, B.; Chang, W. L.; Gordon, M. S.; Dabdub, D.; Gerber, R. B.; Finlayson-Pitts, B. J. Chlorine Activation Indoors and Outdoors via Surface-Mediated Reactions of Nitrogen Oxides with Hydrogen Chloride. *Proc. Natl. Acad. Sci. U.S.A.* **2009**, *106*, 13647−13654.

(11) Jacob, D. J.; Field, B. D.; Li, Q.; Blake, D. R.; de Gouw, J.; Warneke, C.; Hansel, A.; Wisthaler, A.; Singh, H. B.; Guenther, A. Global Budget of Methanol: Constraints from Atmospheric Observations. *J. Geophys. Res.: Atmos.* **2005**, *110*, No. 5172.

(12) Millet, D. B.; Apel, E.; Henze, D. K.; Hill, J.; Marshall, J. D.; Singh, H. B.; Tessum, C. W. Natural and Anthropogenic Ethanol Sources in North America and Potential Atmospheric Impacts of Ethanol Fuel Use. *Environ. Sci. Technol.* **2012**, *46*, 8484−8492.

(13) Luecken, D.; Hutzell, W.; Strum, M.; Pouliot, G. Regional Sources of Atmospheric Formaldehyde and Acetaldehyde, and Implications for Atmospheric Modeling. *Atmos. Environ.* **2012**, *47*, 477−490.

(14) Atkinson, R. Gas-Phase Tropospheric Chemistry of Volatile Organic Compounds: 1. Alkanes and Alkenes. *J. Phys. Chem. Ref. Data* **1997**, *26*, 215−290.

(15) Hui, A. O.; Fradet, M.; Okumura, M.; Sander, S. P. Temperature Dependence Study of the Kinetics and Product Yields of the HO_2 + $CH_3C(O)O_2$ Reaction by Direct Detection of OH and HO_2 Radicals Using 2f-IR Wavelength Modulation Spectroscopy. *J. Phys. Chem. A* **2019**, *123*, 3655−3671.

(16) Moortgat, G.; Veyret, B.; Lesclaux, R. Absorption Spectrum and Kinetics of Reactions of the Acetylperoxy Radical. *J. Phys. Chem.* **1989**, *93*, 2362−2368.

(17) Crawford, M. A.; Wallington, T. J.; Szente, J. J.; Maricq, M. M.; Francisco, J. S. Kinetics and Mechanism of the Acetylperoxy + HO_2 Reaction. *J. Phys. Chem. A* **1999**, *103*, 365−378.

(18) Tomas, A.; Villenave, E.; Lesclaux, R. Reactions of the HO_2 Radical with CH_3CHO and $CH_3C(O)O_2$ in the Gas Phase. *J. Phys. Chem. A* **2001**, *105*, 3505−3514.

(19) Hasson, A. S.; Tyndall, G. S.; Orlando, J. J. A Product Yield Study of the Reaction of HO_2 Radicals with Ethyl Peroxy ($C_2H_5O_2$), Acetyl Peroxy ($CH_3C(O)O_2$), and Acetonyl Peroxy ($CH_3C(O)$-CH_2O_2) Radicals. *J. Phys. Chem. A* **2004**, *108*, 5979−5989.

(20) Le Crâne, J.-P.; Rayez, M.-T.; Rayez, J.-C.; Villenave, E. A Reinvestigation of the Kinetics and the Mechanism of the CH_3C-$(O)O_2$ + HO_2 Reaction Using Both Experimental and Theoretical Approaches. *Phys. Chem. Chem. Phys.* **2006**, *8*, 2163−2171.

(21) Jenkin, M. E.; Hurley, M. D.; Wallington, T. J. Investigation of the Radical Product Channel of the $CH_3C(O)O_2$ + HO_2 Reaction in the Gas Phase. *Phys. Chem. Chem. Phys.* **2007**, *9*, 3149−3162.

(22) Dillon, T. J.; Crowley, J. N. Direct Detection of OH Formation in the Reactions of HO_2 with $CH_3C(O)O_2$ and Other Substituted Peroxy Radicals. *Atmos. Chem. Phys.* **2008**, *8*, 4877−4889.

(23) Groß, C. B. M.; Dillon, T. J.; Schuster, G.; Lelieveld, J.; Crowley, J. N. Direct Kinetic Study of OH and O_3 Formation in the Reaction of $CH_3C(O)O_2$ with HO_2. *J. Phys. Chem. A* **2014**, *118*, 974−985.

(24) Winiberg, F. A. F.; Dillon, T. J.; Orr, S. C.; Grod, C. B. M.; Bejan, I.; Brumby, C. A.; Evans, M. J.; Smith, S. C.; Heard, D. E.; Seakins, P. W. Direct Measurements of OH and Other Product Yields from the HO_2 + $CH_3C(O)O_2$ Reaction. *Atmos. Chem. Phys.* **2016**, *16*, 4023−4042.

(25) Payne, W. A.; Brunning, J.; Mitchell, M. B.; Stief, L. J. Kinetics of the Reactions of Atomic Chlorine with Methanol and the Hydroxymethyl Radical with Molecular Oxygen at 298 K. *Int. J. Chem. Kinet.* **1988**, *20*, 63−74.

(26) Wallington, T. J.; Skewes, L. M.; Siegl, W. O.; Wu, C.-H.; Japar, S. M. Gas Phase Reaction of Cl Atoms with a Series of Oxygenated Organic Species at 295 K. *Int. J. Chem. Kinet.* **1988**, *20*, 867−875.

(27) Nelson, L.; Rattigan, O.; Neavyn, R.; Sidebottom, H.; Treacy, J.; Nielsen, O. J. Absolute and Relative Rate Constants for the Reactions of Hydroxyl Radicals and Chlorine Atoms with a Series of Aliphatic Alcohols and Ethers at 298 K. *Int. J. Chem. Kinet.* **1990**, *22*, 1111−1126.

(28) Dóbé, S.; Otting, M.; Temps, F.; Wagner, H. G.; Ziemer, H. Fast Flow Kinetic Studies of the Reaction CH_2OH + HCl ⇌ CH_3OH + Cl. The Heat of Formation of Hydroxymethyl. *Ber. Bunsen-Ges. Phys. Chem.* **1993**, *97*, 877−883.

(29) Tyndall, G. S.; Orlando, J. J.; Kegley-Owen, C. S.; Wallington, T. J.; Hurley, M. D. Rate Coefficients for the Reactions of Chlorine Atoms with Methanol and Acetaldehyde. *Int. J. Chem. Kinet.* **1999**, *31*, 776−784.

(30) Smith, J. D.; DeSain, J. D.; Taatjes, C. A. Infrared Laser Absorption Measurements of HCl (V = 1) Production in Reactions of Cl Atoms with Isobutane, Methanol, Acetaldehyde, and Toluene at 295 K. *Chem. Phys. Lett.* **2002**, *366*, 417−425.

(31) Seakins, P. W.; Orlando, J. J.; Tyndall, G. S. Rate Coefficients and Production of Vibrationally Excited HCl from the Reactions of Chlorine Atoms with Methanol, Ethanol, Acetaldehyde and Formaldehyde. *Phys. Chem. Chem. Phys.* **2004**, *6*, 2224−2229.

(32) Taketani, F.; Takahashi, K.; Matsumi, Y.; Wallington, T. J. Kinetics of the Reactions of $Cl^*(^2P_{1/2})$ and $Cl(^2P_{3/2})$ Atoms with CH_3OH, C_2H_5OH, n-C_3H_7OH, and i-C_3H_7OH at 295 K. *J. Phys. Chem. A* **2005**, *109*, 3935−3940.

DOI: 10.1021/acs.jpca.9b00038
J. Phys. Chem. A 2019, 123, 4964−4972

(33) Niki, H.; Maker, P. D.; Savage, C. M.; Breitenbach, L. P. FTIR Study of the Kinetics and Mechanism for Chlorine-Atom-Initiated Reactions of Acetaldehyde. *J. Phys. Chem.* **1985**, *89*, 588−591.
(34) Bartels, M.; Hoyermann, K.; Lange, U. An Experimental Study of the Reactions CH_3CHO + Cl, C_2H_4O + Cl, and C_2H_4O + F in the Gas-Phase. *Ber. Bunsen-Ges. Phys. Chem.* **1989**, *93*, 423−427.
(35) Scollard, D. J.; Treacy, J. J.; Sidebottom, H. W.; Balestra-Garcia, C.; Laverdet, G.; LeBras, G.; MacLeod, H.; Teton, S. Rate Constants for the Reactions of Hydroxyl Radicals and Chlorine Atoms with Halogenated Aldehydes. *J. Phys. Chem.* **1993**, *97*, 4683−4688.
(36) Kegley-Owen, C. S.; Tyndall, G. S.; Orlando, J. J.; Fried, A. Tunable Diode Laser Studies of the Reaction of Cl Atoms with CH_3CHO. *Int. J. Chem. Kinet.* **1999**, *31*, 766−775.
(37) Howes, N. U. M.; Lockhart, J. P. A.; Blitz, M. A.; Carr, S. A.; Baeza-Romero, M. T.; Heard, D. E.; Shannon, R. J.; Seakins, P. W.; Varga, T. Observation of a New Channel, the Production of CH_3, in the Abstraction Reaction of OH Radicals with Acetaldehyde. *Phys. Chem. Chem. Phys.* **2016**, *18*, 26423−26433.
(38) Michael, J. V.; Nava, D. F.; Payne, W. A.; Stiefb, L. J. Rate Constants for the Reaction of Atomic Chlorine with Methanol and Dimethyl Ether from 200 to 500 K. *J. Chem. Phys.* **1979**, *70*, 3652−3656.
(39) Lightfoot, P. D.; Veyret, B.; Lesclaux, R. Flash Photolysis Study of the Methylperoxy. Hydroperoxy Reaction between 248 and 573 K. *J. Phys. Chem.* **1990**, *94*, 708−714.
(40) Garzón, A.; Cuevas, C. A.; Ceacero, A. A.; Notario, A.; Albaladejo, J.; Fernndez-Gmez, M. Atmospheric Reactions Cl+CH_3-(CH_2)n-OH (N = 0−4): A Kinetic and Theoretical Study. *J. Chem. Phys.* **2006**, *125*, No. 104305.
(41) Kaiser, E. W.; Wallington, T. J. Rate Constant of the Reaction of Chlorine Atoms with Methanol over the Temperature Range 291−475 K. *Int. J. Chem. Kinet.* **2010**, *42*, 113−116.
(42) Burkholder, J. B.; Sander, S. P.; Abbatt, J.; Barker, J. R.; Huie, R.; Kolb, C. E.; Kurylo, M.; Orkin, V.; Wilmouth, D.; Wine, P. H. In *Chemical Kinetics and Photochemical Data for Use in Atmospheric Studies, Evaluation No. 18*; Jet Propulsion Laboratory, National Aeronautics and Space Administration: Pasadena, CA, 2015.
(43) Atkinson, R.; Baulch, D. L.; Cox, R. A.; Hampson, R. F.; Kerr, J. A.; Troe, J. Evaluated Kinetic and Photochemical Data for Atmospheric Chemistry: Supplement IV. IUPAC Subcommittee on Gas Kinetic Data Evaluation for Atmospheric Chemistry. *J. Phys. Chem. Ref. Data* **1992**, *21*, 1125−1568.
(44) Payne, W. A.; Nava, D. F.; Nesbitt, F. L.; Stief, L. J. Rate Constant for the Reaction of Atomic Chlorine with Acetaldehyde from 210 to 343 K. *J. Phys. Chem.* **1990**, *94*, 7190−7193.
(45) Christensen, L. E.; Okumura, M.; Sander, S. P.; Friedl, R. R.; Miller, C. E.; Sloan, J. J. Measurements of the Rate Constant of HO_2 + NO_2 + N_2 → HO_2NO_2 + N_2 Using Near-Infrared Wavelength-Modulation Spectroscopy and UV-Visible Absorption Spectroscopy. *J. Phys. Chem. A* **2004**, *108*, 80−91.
(46) Noell, A. C.; Alconcel, L. S.; Robichaud, D. J.; Okumura, M.; Sander, S. P. Near-Infrared Kinetic Spectroscopy of the HO_2 and $C_2H_5O_2$ Self-Reactions and Cross Reactions. *J. Phys. Chem. A* **2010**, *114*, 6983−6995.
(47) Grieman, F. J.; Noell, A. C.; Davis-van Atta, C.; Okumura, M.; Sander, S. P. Determination of Equilibrium Constants for the Reaction Between Acetone and HO_2 Using Infrared Kinetic Spectroscopy. *J. Phys. Chem. A* **2011**, *115*, 10527−10538.
(48) Onel, L.; Brennan, A.; Gianella, M.; Ronnie, G.; Lawry Aguila, A.; Hancock, G.; Whalley, L.; Seakins, P. W.; Ritchie, G. A. D.; Heard, D. E. An Intercomparison of HO_2 Measurements by Fluorescence Assay by Gas Expansion and Cavity Ring-down Spectroscopy within HIRAC (Highly Instrumented Reactor for Atmospheric Chemistry). *Atmos. Meas. Tech.* **2017**, *10*, 4877−4894.
(49) *FACSIMILE*; MCPA Software Ltd., 2003.
(50) Atkinson, R.; Baulch, D. L.; Cox, R. A.; Crowley, J. N.; Hampson, R. F.; Hynes, R. G.; Jenkin, M. E.; Rossi, M. J.; Troe, J.; et al. IUPAC Subcommittee, Evaluated Kinetic and Photochemical Data for Atmospheric Chemistry: Volume II - Gas Phase Reactions of Organic Species. *Atmos. Chem. Phys.* **2006**, *6*, 3625−4055.
(51) Christensen, L. E.; Okumura, M.; Hansen, J. C.; Sander, S. P.; Francisco, J. S. Experimental and Ab Initio Study of the HO_2·CH_3OH Complex: Thermodynamics and Kinetics of Formation. *J. Phys. Chem. A* **2006**, *110*, 6948−6959.
(52) Hui, A. O. Atmospheric Peroxy Radical Chemistry Studied by Infrared Kinetic Spectroscopy. Ph.D. Thesis, California Institute of Technology: Pasadena, CA, 2019.
(53) Cruickshank, F. R.; Benson, S. W. Carbon-Hydrogen Bond Dissociation Energy in Methanol. *J. Phys. Chem.* **1969**, *73*, 733−737.
(54) Lee, J.; Bozzelli, J. W. Reaction of H + Ketene to Formyl Methyl and Acetyl Radicals and Reverse Dissociations. *Int. J. Chem. Kinet.* **2003**, *35*, 20−44.
(55) da Silva, G.; Bozzelli, J. W. Enthalpies of Formation, Bond Dissociation Energies, and Molecular Structures of the n-Aldehydes (Acetaldehyde, Propanal, Butanal, Pentanal, Hexanal, and Heptanal) and Their Radicals. *J. Phys. Chem. A* **2006**, *110*, 13058−13067.

DOI: 10.1021/acs.jpca.9b00038
J. Phys. Chem. A 2019, 123, 4964−4972